Available online at www.sciencedirect.com
ScienceDirect
Journal of Power Sources 165 (2007) 293–298
JOURNAL OF POWER SOURCES
www.elsevier.com/locate/jpowsour

Short communication

An investigation into TiN-coated 316L stainless steel as a bipolar plate material for PEM fuel cells

Yan Wang, Derek O. Northwood *

Department of Mechanical, Automotive, and Materials Engineering, University of Windsor, 401 Sunset Avenue, Windsor, Ontario, Canada N9B 3P4

Received 5 October 2006; received in revised form 13 December 2006; accepted 13 December 2006
Available online 28 December 2006

Abstract

In order to reduce the cost, weight and volume of the bipolar plates, considerable attention is being paid to developing metallic bipolar plates to replace the non-porous graphite bipolar plates that are in current use. However, metals are prone to corrosion in the proton exchange membrane (PEM) fuel cell environments, which decreases the ionic conductivity of the membrane and lowers the overall performance of the fuel cells. In this study, TiN was coated on SS316L using a physical vapor deposition (PVD) technology (plasma enhanced reactive evaporation) to increase the corrosion resistance of the base SS316L. X-ray diffraction (XRD), scanning electron microscopy (SEM) and electrochemical methods were used to characterize the TiN-coated SS316L. XRD showed that the TiN coating had a face-centered-cubic (fcc) structure. Potentiodynamic tests and electrochemical impedance tests showed that the corrosion resistance of SS316L was significantly increased in 0.5 M H_2SO_4 at 70 °C by coating with TiN. In order to investigate the suitability of these coated materials as cathodes and anodes in a PEMFC, potentiostatic tests were conducted under both simulated cathode and anode conditions. The simulated anode environment was −0.1 V versus SCE purged with H_2 and the simulated cathode environment was 0.6 V versus SCE purged with O_2. In the simulated anode conditions, the corrosion current of TiN-coated SS316L is -4×10^{-5} A cm^{-2}, which is lower than that of the uncoated SS316L (about -1×10^{-6} A cm^{-2}). In the simulated cathode conditions, the corrosion current of TiN-coated SS316L is increased to 2.5×10^{-5} A cm^{-2}, which is higher than that of the uncoated SS316L (about 5×10^{-6} A cm^{-2}). This is because pitting corrosion had taken place on the TiN-coated specimen.

Keywords: Bipolar plates; PVD; Corrosion; EIS; Coating

1. Introduction

With escalating oil prices and increasing environmental concerns, increasing attention is being paid to the development of fuel cells [1–9]. Fuel cell technology is cleaner, quieter, and more efficient when compared to internal combustion engines [3]. Proton exchange membrane (PEM) fuel cells are regarded as one of the most promising of the fuel cell types for stationary and transportation applications because they operate at low temperatures and allow for rapid start-up [10].

Currently, the non-porous graphite bipolar plates are mainly used because of their chemical and thermal stability. They account for the major portion of the total price, weight and volume of the fuel cell stacks [11]. There is increasing interest being shown to replace the non-porous graphite bipolar plates with metallic bipolar plates and thereby generate weight and cost savings [12]. A number of metallic materials have been investigated including aluminum [13], stainless steel [14,15], titanium [16], nickel [16,17] and a copper alloy [18,19]. However, stainless steel is the only material to have received considerable attention in the non-coated condition [12]. Even for the more corrosion-resistant metallic materials, some researchers [20,21] have reported that metal ions, such as those produced by corrosion of metallic materials, can migrate to the membrane and that levels as low as 5–10 ppm can degrade the membrane performance. Furthermore, any corrosion layer that is formed, will lower the electrical conductivity of the bipolar plates, and thereby increase the potential loss because of a higher electrical resistance.

Physical vapor deposition (PVD) is one of the most promising coating technologies and is widely used for the improvement of the mechanical and corrosion properties of metallic materials

* Corresponding author. Tel.: +1 519 253 3000x4785; fax: +1 519 973 7007.
E-mail address: dnorthwo@uwindsor.ca (D.O. Northwood).

0378-7753/$ – see front matter © 2007 Elsevier B.V. All rights reserved.
doi:10.1016/j.jpowsour.2006.12.034

Table 1
Chemical composition of 316L stainless steel (wt%)

Metal	C	Cr	Ni	Mo	Mn	P	S	Si	Cu	N	Fe
SS316L	0.021	16.32	10.54	2.12	1.82	0.029	0.01	0.58	0.47	0.03	Balance

[22]. TiN coatings have been used in many applications, e.g. cutting tools, because of their high wear resistance, hardness and low friction coefficient characteristics [23]. TiN coatings also have potential application to metallic bipolar plates because of TiN's excellent corrosion resistance and metal-like electrical conductivity [24]. However, little attention has been paid to determining the corrosion performance of TiN coatings on a metallic substrate under actual PEM fuel cell working conditions. In this study, TiN was coated on an austenitic stainless steel (316L) using a PVD technology and the electrochemical characteristics were determined in simulated PEM fuel cell environments. The results are compared with some earlier work on TiN-coated 410 stainless steel [25]. 410 stainless steel is a martensitic stainless steel: martensitic stainless steels are chosen for mechanical strength and their corrosion resistance is lower than other grades of stainless steel [26,27].

2. Experimental details

2.1. PVD coating and electrode preparation

SS316L was chosen as the base material because of its good corrosion resistance. It is generally recognized that the austenitic stainless steels have superior corrosion resistance to other grades of stainless steel such as the ferritic or martensitic [26]. 316SS is one of the more corrosion resistant austenitic stainless steels because of its higher Ni content (10.5 wt%) and the addition of Mo. The 316L grade with its very low C content (0.02 wt%) is also less sensitive to depletion of Cr at the grain boundaries due to carbide precipitation, which can lead to a decrease in corrosion resistance [26,27]. The chemical analysis of the SS316L used in this study is given in the Table 1. The coating process for TiN was plasma enhanced reactive evaporation which is commonly used in such commercial operations as turbine refurbishing.

2.2. Characterization of TiN coatings

The coated samples were examined both by X-ray diffraction (XRD) using a Philips X-ray diffractometer and by scanning electron microscopy (SEM) [JEOL JSM-5800LV].

2.3. Electrochemistry

Potentiodynamic and potentiostatic tests were used to analyze the corrosion characteristics of both uncoated and coated SS316L. Potentiodynamic tests were used to measure the polarization resistance of uncoated and coated SS316L at high (70 °C) temperatures. The electrolyte was a 0.5 M sulphuric acid solution. In order to simulate the working conditions of a PEMFC, potentiostatic tests were conducted under the following conditions: at the anode, the applied potential was −0.1 V versus SCE purged with H_2 and at the cathode, the applied potential was 0.6 V versus SCE purged with O_2 [28]. A Solartron Electrochemical Interface (S1 1287) was used for the electrochemical impedance spectroscopy (EIS) measurements. The impedance measurements were made at the open circuit potential and the perturbation amplitude was 10 mV. The applied frequencies ranged from 1 M to 10^{-1} Hz and the data were analyzed by Zview software.

3. Results and discussion

3.1. XRD for the uncoated and TiN coated SS316L

Fig. 1 presents the XRD results for (a) the uncoated and (b) TiN-coated SS316L. Both the SS316L and TiN have a FCC structure. Comparing Fig. 1a and b, we can see that there are no SS316L peaks for the coated sample since the penetration depth of the X-rays is less than the thickness of the TiN coating. The $(1\,1\,1)_{TiN}$ diffraction peak is the strongest. In the standard TiN diffraction pattern [29] (2 0 0) is the strongest peak and the intensity ratio I_{111}/I_{200} is 0.72. However, the intensity ratio I_{111}/I_{200} for our samples was about 2. Thus, the growth orientation of the TiN was mainly in the ⟨1 1 1⟩ direction, which is consistent with the findings of other researchers [30,31]. The

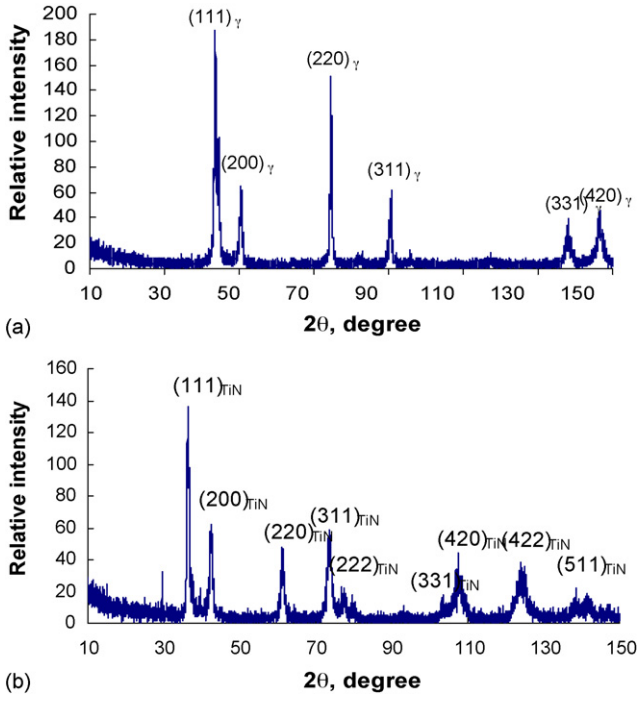

Fig. 1. XRD patterns for uncoated and coated SS316L (a) uncoated SS316, and (b) coated SS316.

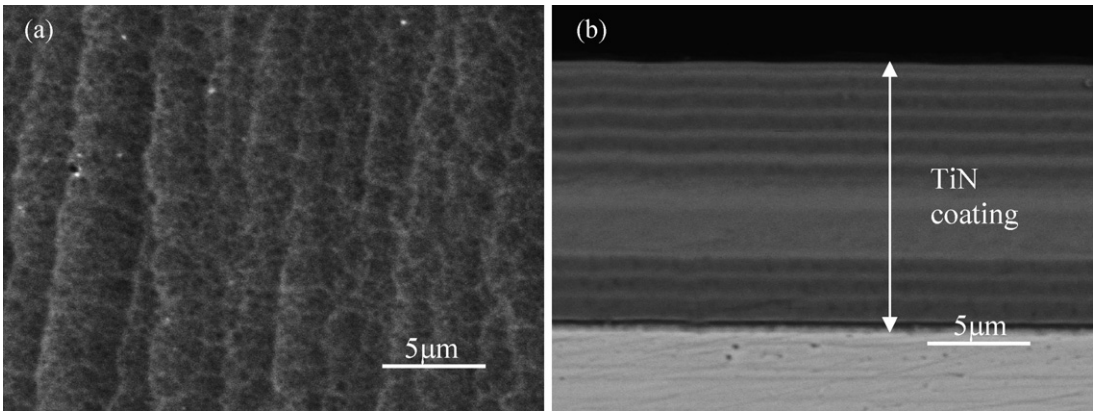

Fig. 2. TiN coated SS316L (a) TiN coating surface (secondary electron image), and (b) cross-sectional view of TiN coating on SS316L (back-scattered electron image).

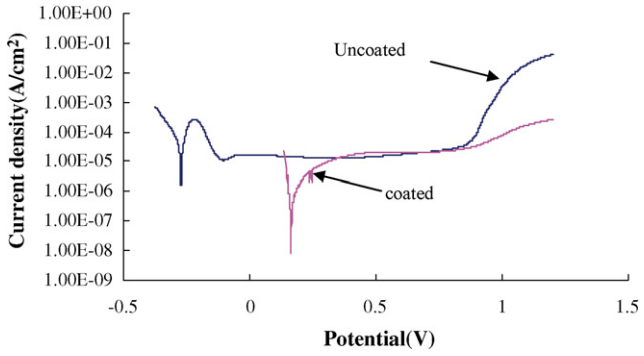

Fig. 3. Potentiodynamic tests for uncoated and TiN-coated SS316L at 70 °C.

XRD pattern for the TiN-coated sample also confirms that the coating is composed solely of FCC structure.

3.2. SEM characterization of TiN coatings

Fig. 2 are SEM micrographs of the TiN coatings on the SS316L surface. Fig. 2a shows that TiN has a 'dented' appearance, due to the columnar growth of the TiN during the coating process. Fig. 2b is a cross-sectional view of the TiN coating, which is 15 μm thick. It is evident from Fig. 2b that the coating is multilayered. This layering has arisen because of regular modulation of the N_2 flow and irregular oscillations of the Ti from the e-beam pool during the commercial coating process. These layers overlap and result in an irregular structure.

3.3. Potentiodynamic testing

Fig. 3 presents the potentiodynamic results for uncoated and coated SS316L. The open circuit potential of the base SS316L is −0.26 V versus SCE. However, the open circuit potential of the TiN-coated SS316L increased to 0.16 V versus SCE. Thus, the increased potential retards corrosion of the base SS316L. Comparing the two curves in Fig. 3, we can see that the base SS316L shows a typical potentiodynamic curve for an austenitic stainless steel, in that it is divided into three regions, namely active, passive and transpassive. However, the corrosion curve for TiN-coated SS316L has no visible transpassive region. In our earlier study of another TiN-coated stainless steel [25], the base martensitic stainless steel (SS410) did not exhibit a passive region at 70 °C, However, the TiN-coated SS410 had almost the same polarization curve as shown here for TiN-coated SS316L. Based on the linear polarization data, we can obtain the polarization resistance of uncoated and coated SS316L at 70 °C:

$$R_p = \frac{\beta_a \beta_c}{2.3 i_{corr}(\beta_a + \beta_c)} \quad (1)$$

where β_a, β_c, i_{corr}, and R_p are the Tafel slopes of the anodic and cathodic reactions, the corrosion current density and polarization resistance, respectively [32].

From Table 2, we can see that the polarization resistance of TiN-coated SS316L is increased by about 30 times, and the corrosion rate is decreased by about 40 times, by coating with TiN. These results are consistent with those for TiN-coated SS410 reported in our earlier paper [25].

Fig. 4 presents SEM micrographs for both uncoated and TiN-coated SS316L after the potentiodynamic tests. From Fig. 4a, we can see that the uncoated SS316L corrodes by grain boundary (intergranular) corrosion. However, from Fig. 4b, we can see that there is no evidence of grain boundary corrosion for the TiN-coated SS316L.

Table 2
Polarization parameters of uncoated and coated SS316L in a 0.5 M sulphuric acid solution at 70 °C

Metal	β_a (V)	β_c (V)	E_{corr} (V)	i_{corr} (μA cm^{-2})	R_p (Ω cm^2)
Uncoated SS316L	0.055	0.074	−0.268	40.318	340
Coated SS316L	0.224	0.026	0.160	1.020	9930

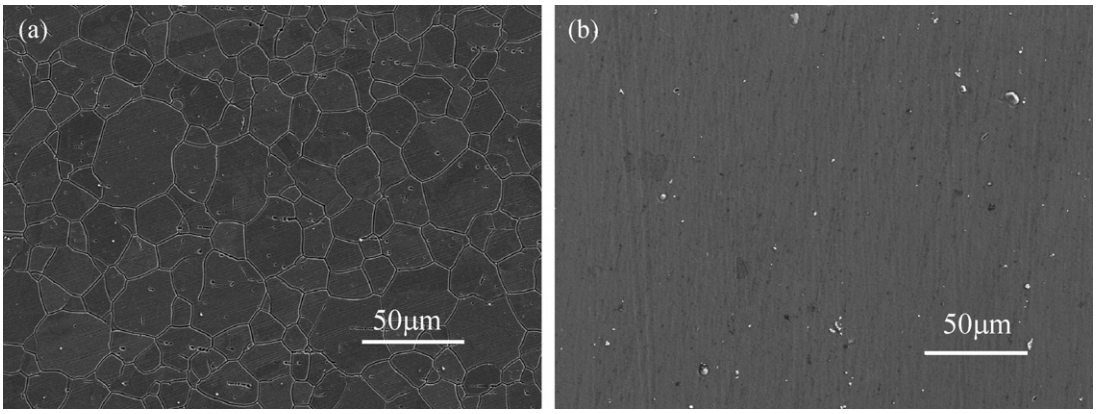

Fig. 4. SEM micrographs for (a) uncoated, and (b) TiN-coated SS316L after potentiodynamic testing.

3.4. Impedance tests

Fig. 5 presents the EIS spectra for uncoated and TiN-coated SS316L. Comparing the two curves in Fig. 4, we can see that the impedance value for TiN-coated SS316L is much higher than that for the uncoated SS316L over the complete curve. This is consistent with the values for the polarization resistance that were obtained in the potentiodynamic tests.

3.5. Potentiostatic testing in simulated anode and cathode conditions

In actual PEMFC working conditions, the anode is at a potential of about −0.1 V versus SCE and the cathode is at a potential of about 0.6 V versus SCE [28]. Because the open circuit potentials of uncoated and TiN-coated SS316L are −0.26 V versus SCE and 0.16 V versus SCE, respectively, the simulated anode potential is anodic to uncoated SS316L and cathodic to TiN-coated SS316L. The simulated cathode potential is anodic to both uncoated and TiN-coated SS316L. Under these PEMFC conditions, any corrosion that takes place is not the same as the free potential corrosion. In order to study the corrosion behavior of metallic bipolar plates in actual PEMFC working conditions, potentiostatic tests were conducted at −0.1 V versus SCE purged with H_2 to simulate the anode working conditions and at 0.6 V versus SCE purged with O_2 to simulate the cathode working conditions. The test results are shown in Fig. 6, for both the simulated cathode and anode conditions.

From Fig. 6a, which is the simulated anode working conditions, we can see that the current density of the uncoated SS316L stabilizes at about -1×10^{-5} A cm^{-2}. For the TiN-coated samples, the current density stabilizes at about -4×10^{-5} A cm^{-2}. This implies that H^+ ions can form H_2 more easily on the TiN-coated surface because TiN has a more positive potential than SS316L. Also, the corrosion current of TiN-coated SS316L became negative immediately after the start of the experiments. However, it took about 50 s for the corrosion current for the base SS316L to become negative. Thus, in the first 50 s, SS316L can corrode in the simulated anode environment. The corrosion current density of TiN-coated SS316L is negative at all

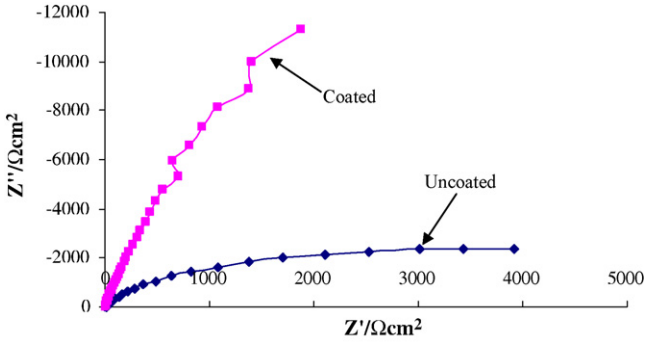

Fig. 5. Electrochemical impedance spectra for the uncoated, and TiN-coated SS316L.

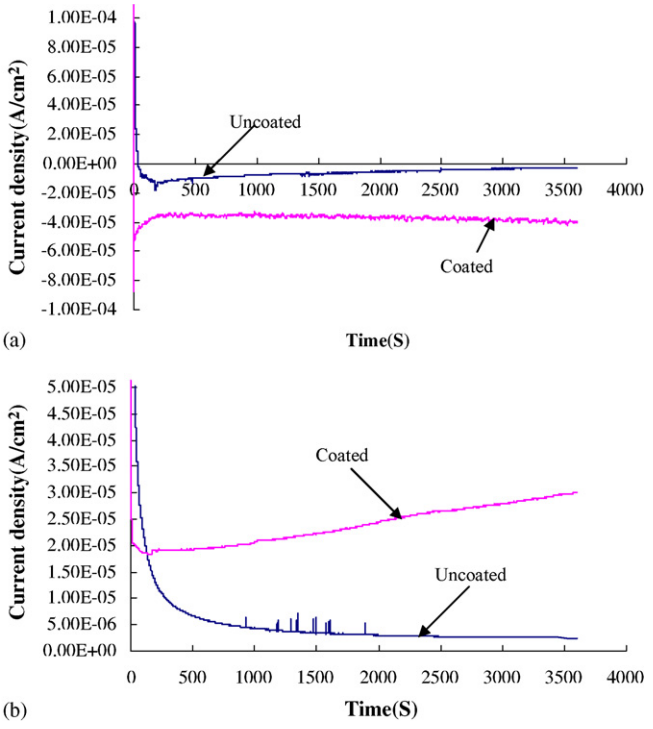

Fig. 6. Potentiostatic tests for the uncoated and TiN-coated SS316L in simulated cathode conditions (a) anode side, and (b) cathode side.

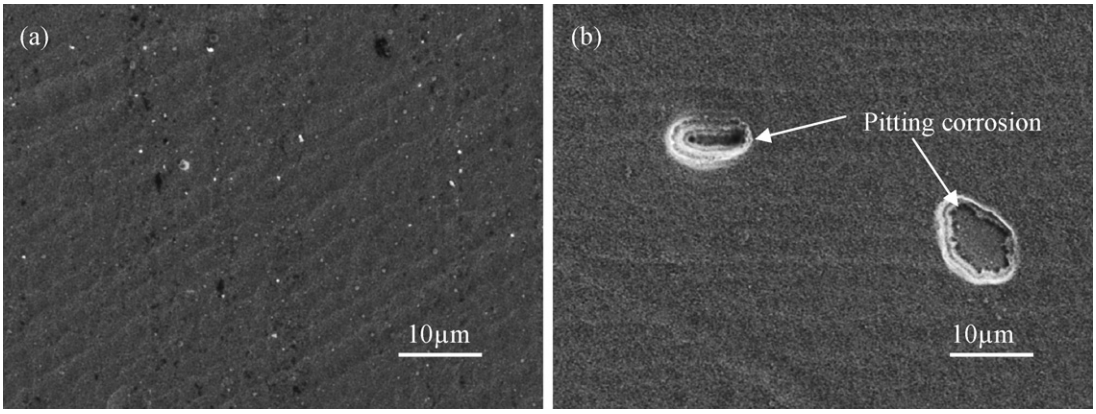

Fig. 7. SEM micrographs for the coated SS316L after potentiostatic tests in the simulated anode and cathode conditions (a) anode side, and (b) cathode side.

times. This negative current provides cathodic protection for both the uncoated and TiN-coated SS316L. Therefore, the TiN-coated SS316L undergoes no corrosion in the simulated anode environment of PEM fuel cells.

Fig. 6b presents the potentiostatic test results for the simulated cathode working conditions. For uncoated samples, the current density is 8×10^{-6} A cm^{-2}, and for the coated samples, the current density stabilizes at about 2.5×10^{-5} A cm^{-2}. It is somewhat surprising that the corrosion current density increased by a factor of about three after coating with TiN. This is because the base SS316L is in the passive region in the simulated cathode environment. Also, the thin TiN coatings, such as those produced by plasma enhanced reactive evaporation, are not 'perfect' and typically contain defects such as pinholes which can give rise to pitting corrosion [31,33,34]. The incidence of these pinhole defects can potentially be reduced through modification of the processing parameters for the plasma enhanced reactive evaporation. Such processing parameter modification would lead to changes in the thickness and chemistry of the TiN-layer. An alternative approach is the use of direct nitriding process, such as plasma nitriding, to produce a dense nitrogen-rich austenitic layer on the surface of the stainless steel [35].

Comparing the present results for TiN-coated SS316L with those for TiN-coated SS410 in our earlier work [25], we find that the corrosion current density for the two materials is almost the same at the simulated cathode side. However, the corrosion current density is of opposite sign at the simulated anode side: the corrosion current density of TiN-coated SS316L is negative, whereas the corrosion current density of TiN-coated SS410 is positive. This is because of the different open circuit potentials (OCP) of the two stainless steels. The OCP of SS316L is about −0.25 V, whereas the OCP of SS410 is about −0.5 V. Our earlier research [36] has demonstrated that H^+ ions more readily form H_2 on the SS316L surface rather than corrosion taking place.

3.6. SEM examination of coated SS316L surfaces after potentiostatic tests in simulated anode and cathode conditions

Fig. 7 presents the SEM micrographs of TiN coated SS316L after potentiostatic testing in the simulated PEM fuel cell working environments. From Fig. 7a, we can see that there is no evidence of corrosion at the anode side. However, there is pitting corrosion at the cathode side. So, if TiN-coated SS316L, fabricated using plasma enhanced reactive evaporation, is used as the bipolar plates of PEMFCs, there will be corrosion problems at the cathode. Methods should be developed to produce improved, i.e. defect-free, TiN coatings to prevent pitting corrosion.

4. Conclusions

TiN was successfully coated on SS316L and the coatings were about 15 μm thick. The open circuit potential of the TiN-coated SS316L increased to 0.16 V versus SCE from −0.26 V versus SCE for the base SS316L. The TiN-coating increased the polarization resistance by a factor of 30 and reduced the corrosion current density by a factor of 40. EIS showed that the electrochemical impedance of TiN-coated SS316L was considerably higher than for uncoated SS316L, which is consistent with the polarization resistance measurements from the potentiodynamic tests. In the simulated anode environment, the corrosion current density of TiN-coated SS316L immediately becomes negative, which would provide cathodic protection to the metallic bipolar plates. In the simulated cathode environment, the TiN-coating increased the measured corrosion current density because of the presence of pitting corrosion. Therefore, the cathode side will have corrosion problems if TiN-coated SS316L is used for the bipolar plates of PEM fuel cells. Improved TiN coatings, which do not contain defects such as pinholes, are required if TiN-coated SS316L is to be used to fabricate bipolar plates, particularly for use the cathode environment.

Acknowledgements

The authors wish to thank Mr. John Robinson for his assistance with the XRD and SEM examination. The research was financially supported by the Natural Sciences and Engineering Research Council of Canada (NSERC) through a Discovery Grant awarded to Prof. D.O. Northwood.

References

[1] D.A. Boysen, T. Uda, C.R.I. Chisholm, S.M. Haile, Science 303 (2004) 68–70.
[2] Z. Zhan, S.A. Barnett, Science 308 (2005) 844–847.
[3] R.W. Lashway, MRS Bull. 30 (2005) 581–583.
[4] R.G. Rajendran, MRS Bull. 30 (2005) 587–590.
[5] T.A. Morris, E.A. Barringer, S.C. Kung, R.W. Mckain, MRS Bull. 30 (2005) 596–600.
[6] M. Farooque, C. Yuh, H.C. Maru, MRS Bull. 30 (2005) 602–606.
[7] N.P. Brandon, S. Skinner, B.C.H. Steele, Annu. Rev. Mater. Res. 33 (2003) 183–213.
[8] X. Li, I. Sabir, Int. J. Hydrogen Energy 30 (2005) 359–371.
[9] V. Mehta, J.S. Cooper, J. Power Sources 114 (2003) 32–53.
[10] D.P. Davies, P.L. Adcock, M. Turpin, S.J. Rowen, J. Appl. Electrochem. 30 (2000) 101–105.
[11] H. Tauchiya, O. Kobayashi, Int. J. Hydrogen Energy 29 (2004) 985–990.
[12] A. Hermann, T. Chaudhuri, P. Spagnol, Int. J. Hydrogen Energy 30 (2005) 1297–1302.
[13] J. Wind, R. Spah, W. Kaiser, G. Bohm, J. Power Sources 105 (2002) 256–260.
[14] S.-J. Lee, C.-H. Huang, J.-J. Lai, Yu-P. Chen, J. Power Sources 131 (2003) 243–257.
[15] H. Wang, M.A. Sweikart, J.A. Turner, J. Power Sources 115 (2003) 243–257.
[16] I. Zafar, J. Guiheen, N. Dave, R. Timothy, World Patent WO00128019 (19 April 2001).
[17] T. Matsumoto, J. Niikura, H. Ohara, M. Uchida, H. Gyoten, K. Hatoh, E. Kanbara, K. Nishida, Y. Sugawara, European Patent EP 1094535 (25 April 2001).
[18] V.V. Nikam, R.G. Reddy, J. Power Sources 152 (2005) 146–155.
[19] V.V. Nikam, R.G. Reddy, Int J. Hydrogen Energy 31 (2006) 1863–1873.
[20] L. Ma, S. Warthesen, D.A. Shores, J. New Mater. Electrochem. Syst. 3 (2000) 221–228.
[21] M.P. Brady, K. Weisbrod, I. Paulauskas, R.A. Buchanan, K.L. More, H. Wang, M. Wilson, F. Garzon, L.R. Walker, Scripta Mater. 50 (2004) 1017–1022.
[22] L.A. Dobrzański, K. Lukaszkowicz, A. Zarychta, L. Cunha, J. Mater. Process. Technol. 164–165 (2005) 816–821.
[23] Y. Li, L. Qu, F. Wang, Corros. Sci. 45 (2003) 1367–1381.
[24] M. Li, S. Luo, C. Zeng, J. Shen, H. Lin, C. Cao, Corros. Sci. 46 (2004) 1369–1380.
[25] Y.Wang, D.O.Northwood, An Investigation on PVD TiN-Coated SS410 for application as a bipolar plate material for PEM Fuel Cells, Int. J. Hydrogen Energy, submitted for publication.
[26] D.A. Jones, Principles and Prevention of Corrosion, second ed., Prentice Hall, Upper Saddle River NJ, 1996, p. 518.
[27] J.T.N. Atkinson, H. VanDroffelaar, Corrosion and its Control, National Association of Corrosion Engineers, Houston, 1982, p.179.
[28] H. Wang, J.A. Turner, J. Power Sources. 128 (2004) 193–200.
[29] W. Wong, H. McMurdie, B. Paretzkin, C. Hubbard, A. Dragoo, Powder Diffr. 2 (1987) 191–202.
[30] C. Hsu, M. Chen, K. Lai, Mater. Sci. Eng. A 421 (2006) 182–190.
[31] H.C. Barshilia, M.S. Prakash, A. Poojari, K.S. Rajam, Thin Solid Films 460 (2004) 133–142.
[32] D.A. Jones, Principles and Prevention of Corrosion, first ed., Macmillan, New York, 1992, p. 147.
[33] F. Lang, Z. Yu, Surf. Coat. Technol. 145 (2001) 80–87.
[34] H.A. Jehn, Surf. Coat. Technol. 125 (2000) 212–217.
[35] R. Tian, J. Sun, L. Wang, Int. J. Hydrogen Energy 31 (2006) 1874–1878.
[36] Y. Wang, D.O. Northwood, An electrochemical investigation of potential metallic bipolar plate materials for PEM fuel cells, in: Presented at International Symposium on Solar-Hydrogen-Fuel Cells, Cancun, Mexico, August 20–24, 2006.